

Research Article

Open Access



Adaptive robust control for biped walking under uncertain external forces

Helin Wang, Qijun Chen

Department of Control Science and Engineering, Tongji University, Shanghai 201804, China.

Correspondence to: Prof. Qijun Chen, Department of Control Science and Engineering, Tongji University, No.4800 Cao'an Road Jiading District, Shanghai 201804, China. E-mail: qjchen@tongji.edu.cn

How to cite this article: Wang H, Chen Q. Adaptive robust control for biped walking under uncertain external forces. *Intell Robot* 2023;3(3):479-94. <http://dx.doi.org/10.20517/ir.2023.26>

Received: 30 May 2023 **First Decision:** 8 Aug 2023 **Revised:** 20 Aug 2023 **Accepted:** 11 Sep 2023 **Published:** 27 Sep 2023

Academic Editor: Hongtian Chen, Simon X. Yang **Copy Editor:** Dan Zhang **Production Editor:** Dan Zhang

Abstract

Adaptability and robustness are important expressions of the intelligent walking ability of biped robots. This paper is concerned with the problem of dynamical biped walking and robust control of biped robots under external forces. Due to the characteristics of strong coupling and hybrid, the robotic system is modeled as a rigid kinematic chain with Lagrange equations. A novel adaptive feedback controller is proposed based on sliding mode control (SMC) and hybrid zero dynamics. The novelty of the proposed work lies in taking the uncertainty of upper-bound error into consideration. The hybrid robust control is mentioned to approximate unknown dynamic functions with the adaptive weight. The restricted Poincare return map is utilized to analyze the stability of a nonlinear impulsive system. It ensures that the flow of the continuous subsystem can pass through the impact cross section. Finally, the simulation results illustrate that the proposed adaptive SMC control system can favorably track the reference trajectories, even when a fault occurs, which verifies the effectiveness of the proposed method.

Keywords: Biped walking, impulse hybrid system, adaptive sliding mode control, stability analysis

1. INTRODUCTION

Recently, intelligent robots reflect the deep integration of new-generation information technologies, such as intelligent control and high-performance computing, and stand for major direction for the development of the new-generation artificial intelligence strategy of the country. As the ultimate form of intelligent robots, hu-



© The Author(s) 2023. **Open Access** This article is licensed under a Creative Commons Attribution 4.0 International License (<https://creativecommons.org/licenses/by/4.0/>), which permits unrestricted use, sharing, adaptation, distribution and reproduction in any medium or format, for any purpose, even commercially, as long as you give appropriate credit to the original author(s) and the source, provide a link to the Creative Commons license, and indicate if changes were made.



manoid robots require complex mechanical control systems, environmental awareness, and motion planning capabilities, which are widely used in service entertainment, disaster rescue, rehabilitation medicine, and so on^[1-3]. Specially, flexible and robust walking is the most basic guarantee for various tasks. However, uncertain disturbances are inevitable in biped walking, which can affect walking stability or even periodic motion. Hence, it is of great significance to explore advanced high-performance robot control systems, break through the application bottleneck for fieldwork robots, and promote the development of humanoid robots.

Stability analysis is a convincing demonstration of robust walking. By analyzing the conditions for the existence of stable equilibrium points, the stability analysis will transform into a mathematical problem for the existence of limit cycles. Various stability criteria have been proposed. Early scholars proposed the zero moment point (ZMP) stability criterion, which means that the robot is considered stable when the ZMP falls within the support area. Goswamiti designed a sole flipping indicator^[4]. Huang further discussed the determination of the stable region^[5], and then a large number of 3D bipedal solid robots were manufactured based on this criterion. However, a series of problems arose subsequently, such as stiff movement and poor anti-interference ability. Considering stable bipedal walking exhibits periodic motion, the restricted Poincare Return Map can be used to analyze the stability of the system, which transforms the target of stable biped walking into the problem of stabilization of periodic orbits. The main purpose of using the Poincare return map is to analyze the stability of periodic orbits in low dimensions. Besides, it is not constrained by motion speed and, thus, is suitable for various foot structures. Tedrake analyzed the walking stability of a partially passive robot with drive only at the ankle joint^[6]. Grizzle et al. developed new jumping and running postures for point-legged robots^[7].

Compared to the walking ability of humans, biped robots still have a long way to go. They can be regarded as multi-variable, variable structure, and strong coupling nonlinear systems, possessing the characteristics of strong environmental adaptability, complex structure, and difficult motion control^[8-11]. Recent years have witnessed the rapid development of robust control of dynamic biped walking. The traditional quasi-static walking control based on ZMP has practicability; however, it is required that ZMP always falls in the support polygon, which is inconsistent with human walking^[12-14]. For the dynamic walking of biped robots under external forces, Ames^[14] proposed a hybrid zero dynamics control method and gave the analytical conditions for stable dynamic walking. Since SMC is insensitive to parameter changes and disturbances and has a fast response, it has become a research focus for robot control. Active force control is achieved by adding sensors to detect the external forces on the robot and designing corresponding force control algorithms to achieve the robot's active compliance with external forces. The classical force control usually includes impedance control and hybrid position and force control. Yadukumar et al. achieved the robot AMBER walking by collecting and analyzing human gait data and combining it with hybrid zero dynamics^[15]. The classic force control strategy is applicable to static environments in which environmental information is determined. The foundation of force control is the perception of external forces. There are generally two ways to measure external forces: one is to directly obtain the interaction force with the environment through external sensors; Another approach is to use the dynamic model of the robot to obtain external forces. Dai et al. took the ground as an external disturbance, quantified the robustness of the robot to ground disturbances through gain L2, and realized the robot's walking based on robust control^[16].

In the references^[17-20], the control method of a second-order sliding mode is introduced systematically, including a twisting algorithm, sub-optimal algorithm, and terminal sliding mode algorithm. Then, a motion/force hybrid control method based on recurrent neural networks (RNNs) was proposed afterward. Spong et al. proposed a continuous controller design method for dynamic walking on the uneven road^[21]. However, it is difficult to adjust control parameter items. Ravichandran et al. proposed a neural network control method with the inverted pendulum model^[22]. In view of the strong approximation ability of neural networks, they are usually utilized to approximate complex nonlinear systems. Particularly, combining with the self-adaptive tech-

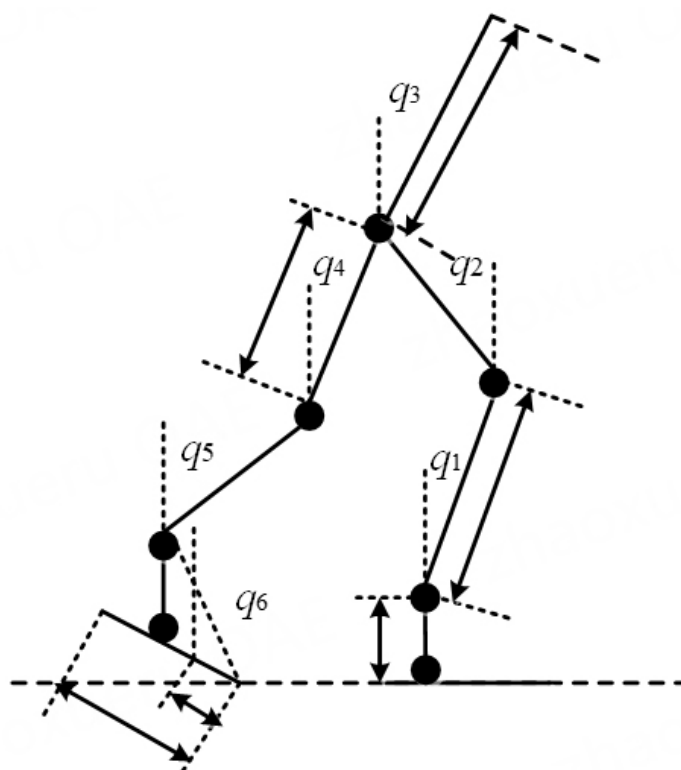


Figure 1. The nine-link model of biped robots.

nology, network weight coefficient identification and updating learning factors can be realized. It has a good generalization ability and can approach any nonlinear function with the required accuracy, which is suitable for real-time and online control of signal processing and robot control [23–26]. Although there are numerous advanced results on biped dynamic walking [27,28], there are still some unresolved issues worth studying, such as the robustness of walking and mobility flexibility. In this paper, we concentrate on adaptive robust control for bipedal robots under uncertain external forces.

The main content of the article is arranged as follows. Section 2 describes the dynamic model of the biped robot. It is modeled as a nonlinear impulsive system. An adaptive sliding-mode controller is proposed in Section 3. In Section 4, a primary RNN with self-stabilizing ability is utilized to deal with the complicated optimization problem. The hybrid robust control is then proposed to approximate unknown dynamic functions, and the network weights are adaptive. The simulation results are shown in Section 5, and Section 6 further proposes future work.

2. DYNAMIC MODELS

The biped robot model discussed in this paper is depicted in Figure 1, which includes a torso and two legs with revolute knees. $q = [q_1, q_2, q_3, q_4, q_5, q_6]^T$ represents the angle of each joint. According to geometrical constraints on the biped robot joint coordinates, the constraints in the double-support phase are holonomic.

Assumption 2.1. The swinging foot and the ground are completely elastic collisions.

Assumption 2.2. The joint angle remains the same, while the angular velocity changes immediately since the impact occurs instantaneously.

Assumption 2.3. The swinging leg did not slip or rebound with the ground during the collision.

Remark 1: The Assumptions 2.1-2.3 are general. These assumptions make it necessary to establish a relationship between the walking process and the dynamic model. Additionally, these assumptions have also been used in [29,30].

The motion equation in the double support phase is described as,

$$M(q)\ddot{q} + C(q, \dot{q})\dot{q} + G(q) = D(u + u_d) \tag{1}$$

where $M(q) \in R^{n \times n}$ is the positive-definite inertia matrix, $G(q) = \partial P / \partial q \in R^n$ is the gravity matrix, and $J = \partial \Phi / \partial q \in R^n$ is the Jacobian matrix. Φ represents robot constraints, and $\Phi(q) = 0$. The nonlinear dynamic equation of the biped robot can be described as a second-order differential equation. $C(q, \dot{q}) \in R^{n \times n}$ is the centrifugal force and Coriolis force terms, and

$$\begin{cases} C(q, \dot{q})\dot{q} = \frac{\partial}{\partial q}(M(q)\dot{q})\dot{q} - \frac{1}{2}(M(q)\dot{q})'\dot{q} \\ C_{kj} = \sum_{i=1}^N \frac{1}{2} \left(\frac{\partial M_{kj}}{\partial q_i} + \frac{\partial M_{ki}}{\partial q_j} - \frac{\partial M_{ij}}{\partial q_k} \right), \quad k \geq 1, j \leq N \end{cases} \tag{2}$$

where N is the length of the generalized configuration vector. $u \in R^n$ is the input torques, and $u_d \in R^n$ is the external disturbance. Considering the external force exerted on the robot foot during an impact, which is defined as $F_{ext} = \int_{t^-}^{t^+} \delta F_{ext}(\tau) d(\tau)$, (1) can be described as

$$\begin{cases} M_e(q_e)\ddot{q}_e + C_e(q_e, \dot{q}_e)\dot{q}_e + G_e(q_e) = \tau + \delta F_{ext} \\ M_e(\dot{q}_e^+) \dot{q}_e^+ - M_e(\dot{q}_e^-) \dot{q}_e^- = F_{ext} \end{cases} \tag{3}$$

where $q_e = [q_1 \quad q_2 \quad p_x \quad p_y]^T$, and (p_x, p_y) shows the hip position in Cartesian coordinates. $M_e(q_e)$, $C_e(q_e)$, and $G_e(q_e)$ are inertia matrix, Coriolis force matrix, and gravity matrix in the double support phase, respectively. The collision mapping can be written as

$$\begin{cases} q^+ = q^- \\ \dot{q}^+ = \Delta(\dot{q}^-) \end{cases} \tag{4}$$

Describing (2) and (4) as the form of state space, as shown in (5), demonstrates that the walking system is hybrid.

$$\Sigma : \begin{cases} \dot{x}(t) = (f(x(t)) + \Delta f(x(t))) + (g(x(t)) + \Delta g(x(t)))u(t) & x(t) \in D \setminus S \\ x^+(t) = \Delta(x^-(t)) & x^-(t) \in S \end{cases} \tag{5}$$

where $x(t) = [q, \dot{q}]^T$ is the defined state variable, and $x^-(t) = [q^-, \dot{q}^-]^T$ and $x^+(t) = [q^+, \dot{q}^+]^T$ represent state variables before and after the impact, respectively. $f(x(t))$ and $g(x(t))$ are bounded nominal nonlinear functions; $\Delta f(x(t))$ and $\Delta g(x(t))$ represent uncertainties. Through differential homeomorphism transformation, the continuous part of the hybrid system (5) can be expressed as a nonlinear system with uncertainties,

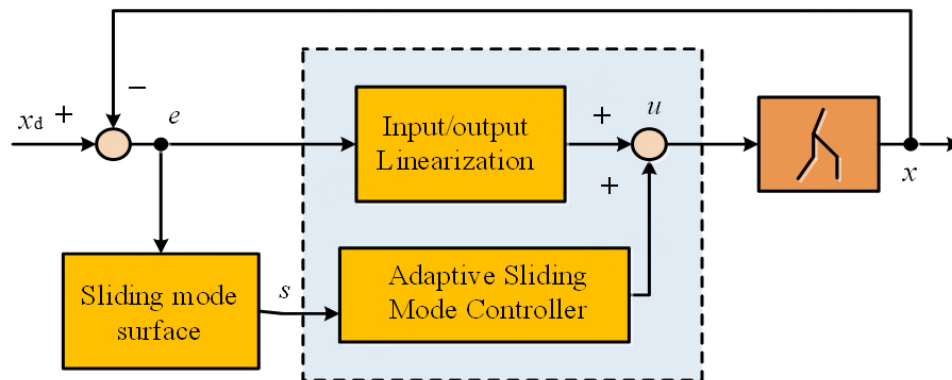


Figure 2. Basic principle diagram of adaptive sliding mode control (SMC).

$$\dot{x}(t) = f(x(t)) + g(x(t))u(t) + \delta(x(t)) \tag{6}$$

where $\delta(x(t))$ is the system uncertainty, which includes system model uncertainties and external disturbances. Suppose $\delta(x(t))$ is bounded; that is, $\|\delta(x(t))\| \leq \rho$, where $\|\cdot\|$ is the Euclid norm, and ρ is a positive constant.

3. ADAPTIVE SLIDING MODE CONTROL

An adaptive sliding mode controller for uncertain disturbances is proposed in this section. The control system block diagram is shown in Figure 2. The basic control idea is to design a sliding mode controller, which makes the state of the system converge to the sliding mode surface when the robot is subjected to uncertain disturbances. In general, the controller design can be divided into two steps. A sliding surface is established to make the controlled system reach its control target.

Due to the adaptability of error amplitude, the controller does not need to accurately estimate the amplitude of external disturbance. Let $\Delta q = q - q_d$ describe the joint control error, where q_d is the reference track of each joint. Thus, the control target can be expressed as $s = \Delta \dot{q} + \alpha \Delta q \rightarrow 0$. However, in the actual robot operation, it will lead to chattering. In order to guarantee smooth operation, the regularization method in the boundary layer is utilized to solve the chattering problem. A controller is designed to make the state trajectory of the robot converge to a thin boundary layer, which is about the constant $\rho = \{(q, \dot{q}) \mid \|s\| < \Phi I_{8 \times 1}\}$; that is to say, for $\forall i > 0$, the robot will meet the following sliding mode conditions when $|s| > \Phi$, and

$$\frac{1}{2} \frac{d}{dt} s_i^2 = \dot{s}_i s_i < 0$$

Considering the coefficients of the Hurwitz polynomial $c_1 + c_2 \lambda + \dots + c_{n-1} \lambda^{n-2} + \lambda^{n-1}$, the sliding mode function can be selected as

$$s_i(t) = e^{(n-1)}(t) + \alpha_1 e^{(n-2)}(t) + \dots + \alpha_{n-1} e(t) + \alpha_n \int_0^t e(t) dt \tag{7}$$

where the constants $c_l (l = 1, 2, \dots, n - 1)$ are to be selected to meet the requirement of sliding surface, and the derivative of s about time t is

$$\begin{aligned}\dot{s}_i(t) &= e^{(n)}(t) + c_1 e^{(n-1)}(t) + \dots + c_{n-1} \dot{e}(t) + c_n e(t) \\ &= \alpha^T E(t) + \beta \dot{E}(t)\end{aligned}\quad (8)$$

where $\alpha = [\alpha_n \ \alpha_{n-1} \ \dots \ \alpha_{n-1}]^T$, $\beta = [0 \ 0 \ \dots \ I]^T$, and $E(t) = [e^T(t) \dot{e}^T(t) \ \dots \ e^{(n-1)T}(t)]$ will converge to the origin when $s_i = 0$.

For a nonlinear system with bounded uncertainties (6), the designed sliding mode controller is proposed to ensure the system is asymptotically stable. It includes two parts: the former is used to realize input/output linearization, and the latter is used for robust compensation. The control law is designed as (9),

$$u_{SMC}(t) = g^{-1}(x(t)) \left[-f(x(t)) + x_d^{(n)}(t) + \alpha^T E(t) + \rho \operatorname{sgn}(s(t)) \right] \quad (9)$$

where $\operatorname{sgn}(\cdot)$ is the sign function. A simple proof of convergence of the controller is as follows. Firstly, taking the splitting operation of the control law (9),

$$u_{SMC}(t) = g^{-1}(x(t)) \left[-f(x(t)) + x_d^{(n)}(t) + \alpha^T E(t) \right] + g^{-1}(x(t)) \rho \operatorname{sgn}(s(t)) \quad (10)$$

Substitute the control law (11) into the nonlinear system (7); it will be denoted by

$$\begin{aligned}x^{(n)}(t) &= f(x(t)) + g(x(t))u_{SMC}(t) + \delta(x(t)) \\ &= f(x(t)) - f(x(t)) + x_d^{(n)}(t) + \alpha^T E(t) + \rho \operatorname{sgn}(s(t)) + \delta(x(t)) \\ &= x_d^{(n)}(t) + \alpha^T E(t) + \rho \operatorname{sgn}(s(t)) + \delta(x(t))\end{aligned}\quad (11)$$

thus, it can get $\rho \operatorname{sgn}(s(t)) + \delta(x(t)) = -\alpha^T E(t) - \beta \dot{E}(t) = -\dot{s}(t)$.

The Lyapunov method is utilized to verify the stability of the control system. We select the candidate Lyapunov function as follows:

$$V_s(s(t)) = \frac{1}{2} s^T(t) s(t) \quad (12)$$

By taking the derivative of $V_s(s(t))$ with respect to t , it follows that

$$\begin{aligned}\dot{V}_s(s(t)) &= s^T(t) \dot{s}(t) \\ &= -s^T(t) [\rho \operatorname{sgn}(s(t)) + \delta(x(t))] \\ &= -\rho \|s(t)\| - s^T(t) \delta(x(t)) \\ &\leq -\rho \|s(t)\| + \|s(t)\| \|\delta(x(t))\| \\ &= -\|s(t)\| (\beta - \delta(x(t)))\end{aligned}\quad (13)$$

According to the assumption that $\delta(x(t))$ is bounded, where $\|\delta(x(t))\| \leq \rho$, so that $\dot{V}_s(s(t)) \leq 0$. Therefore, the SMC law (9) can make the robot system (6) asymptotically stable.

4. HYBRID MOTION/ FORCE CONTROL BASED ON RNN

Considering the uncertainty of the upper-bound error in the controller, a primary RNN is utilized. By designing adaptive laws of network weights based on the Lyapunov stability theory, the parameters of learning factors in neural networks are adjusted. In addition, the boundary value estimation algorithm is utilized to compensate for the estimation error. In order to analyze the system stability, the Poincare return map is utilized, in which the manifold of a continuous subsystem can pass through the impact cross section.

4.1. Principle and structure of RNN

A primary RNN is adopted to deal with the complicated optimization problem. It will remember previous information and use it to affect the output of subsequent nodes. The mapping equation of an RNN is expressed as follows:

$$\dot{V}_{ir}(t) = \sum_{i=1}^n w_j \phi_j (\|x_i(t) - v_{ij}\|, \sigma_{ij}, r_j, \phi_j(t - 1)) \tag{14}$$

where x_i represent input variables, x_{ir} are output variables, w_i is denoted by connective weights between the hidden layer and output layer, and v_{ij} and σ_{ij} are the center and the width of the Gaussian function - j th block membership function - in the i th input. r_j is the internal feedback gain. The base function of the j th block acceptance field corresponding to the i th input x_i can be written as

$$\phi_j(t) = \exp \left[- \sum_{i=1}^m \frac{[x_i(t) + \phi_j(t - 1)r_j - v_{ij}]^k}{\sigma_{ij}^2} \right], \tag{15}$$

The k th multidimensional acceptance domain function and the corresponding multidimensional domain space are respectively denoted by

$$\begin{cases} \Phi_k = \prod_{i=1}^n \phi_{A_{ik}}(x_i) = \exp \left[\sum_{i=1}^n \frac{(x_i - m_{ik})^2}{\sigma_{ik}^2} \right], k = 1, 2 \dots n_R, \\ \Phi = [\Phi_1 \quad \Phi_2 \dots \Phi_{n_R}]^T \end{cases} \tag{16}$$

where n_R is the number of receptive fields.

Define the weight memory space matrix $W = [w_1 \quad w_2 \dots w_i \dots w_{n_R}]^T$, where $w_i = [w_{i1} \quad w_{i2} \dots w_{im}]^T$. Then, the coverage of multidimensional function space Φ to the input state I will also change. The output of the system Y is the product of the weight matrix W and the vector of the receptive field Φ , which can be described in the form of $Y = [y_1 \quad y_2 \quad \dots \quad y_m] = W^T \Phi$.

4.2. Design of a hybrid force/motion controller

The control structure of a hybrid motion/force controller is shown in Figure 3. In order to derive optimized contact force and motion, hybrid motion/force control is proposed based on RNNs to approximate dynamic functions. Several assumptions are made in advance.

Assumption 4.1. According to the approximation principle of neural networks, suppose that there exists the desired weight W^* , Gauss function Φ^* , desired center value m^* , width σ^* , and recurrent gain coefficient r^* , which makes an RNN approach any smooth nonlinear function δ .

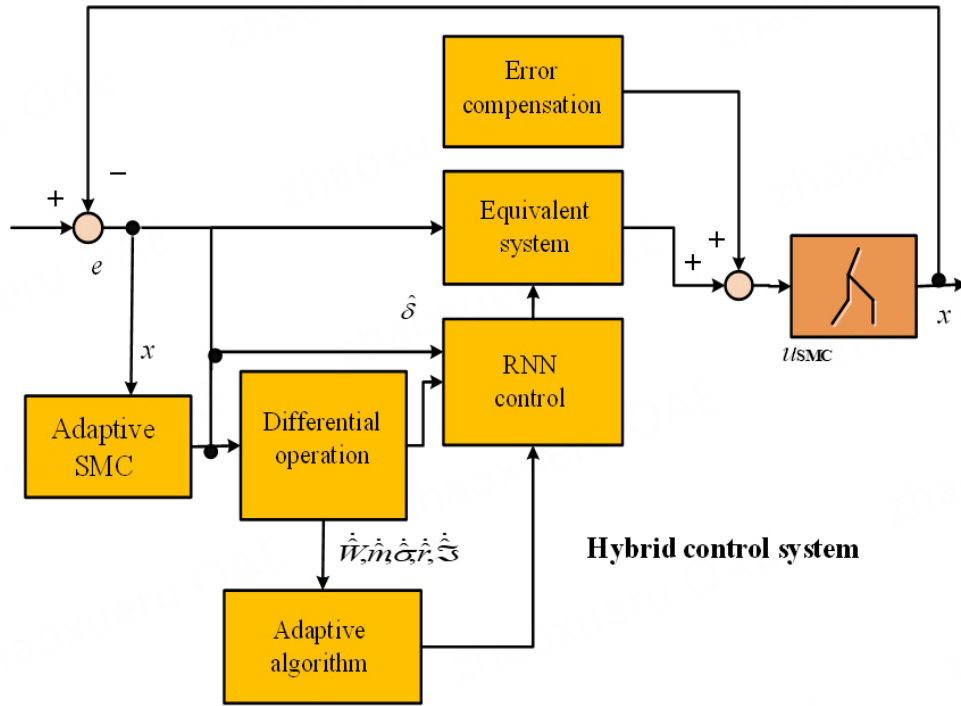


Figure 3. The control structure.

$$\delta = \delta^* + \xi = W^* \Phi^* (m^*, \sigma^*, r^*) + \xi, \tag{17}$$

where $W^*, \Phi^*, m^*, \sigma^*, r^*$ are the desired values of network parameters - W, Φ, m, σ, r . Suppose that $W^*, \Phi^*, m^*, \sigma^*, r^*$ are all bounded, $\|W^*\| \leq \bar{W}, \|\Phi^*\| \leq \bar{\Phi}, \|m^*\| \leq \bar{m}, \|\sigma^*\| \leq \bar{\sigma},$ and $\|r^*\| \leq \bar{r}$. $\bar{W}, \bar{\Phi}, \bar{m}, \bar{\sigma}, \bar{r}$ are the corresponding upper bound of each parameter, and ξ is the approximation error, which satisfies $\|\xi^*\| \leq \bar{\xi}$. However, the desired values $W^*, \Phi^*, m^*, \sigma^*, r^*, \delta^*$ are not available.

Inspired by pure-motion tracking, some notations are defined as ,

$$\begin{aligned} x^{(n)} &= f(x) + g(x)u + \hat{\delta} \\ \hat{\delta} &= \hat{W} \hat{\Phi}(\hat{m}, \hat{\sigma}, \hat{r}) \end{aligned} \tag{18}$$

where $\hat{W}, \hat{\Phi}, \hat{m}, \hat{\sigma}, \hat{r}$ are the estimated values of $W^*, \Phi^*, m^*, \sigma^*, r^*$. $\hat{\delta}$ is the estimation of the system error.

By adjusting the adaptive parameters of RNNs, the hybrid motion/force controller will approximate unknown dynamic functions. From the part of error estimation $\hat{\delta} = \hat{W} \hat{\Phi}(\hat{m}, \hat{\sigma}, \hat{r})$, the error is defined by

$$\begin{aligned} \tilde{\delta} &= \delta - \hat{\delta} = \delta^* + \xi - \hat{\delta} \\ &= W^{*T} \Phi^* - \hat{W}^T \hat{\Phi} + \xi \\ &= W^{*T} \Phi^* - (W^* - \tilde{W})^T (\Phi^* - \tilde{\Phi}) + \xi, \\ &= W^{*T} \tilde{\Phi} - \tilde{W}^T \Phi^* + \tilde{W}^T \tilde{\Phi} + \xi \\ &= \tilde{W}^T \tilde{\Phi} + (\tilde{W}^T + \hat{W}^T) \tilde{\Phi} + \xi \\ &= \tilde{W}^T \tilde{\Phi} + \tilde{W}^T \tilde{\Phi} + \hat{W}^T \tilde{\Phi} + \xi \end{aligned} \tag{19}$$

where $\tilde{W} = W^* - \hat{W}$, and $\tilde{\Phi} = \Phi^* - \hat{\Phi}$.

Utilizing with the Taylor expansion of nonlinear functions, we can get that

$$\tilde{\Phi} = \Phi_m \tilde{m} + \Phi_\sigma \tilde{\sigma} + \Phi_r \tilde{r} + o(\cdot). \tag{20}$$

Substituting (20) into (19), we get

$$\begin{aligned} \tilde{\delta} &= \tilde{W}^T \tilde{\Phi} + \tilde{W}^T \hat{\Phi} + \hat{W}^T \tilde{\Phi} + \xi \\ &= \tilde{W}^T \tilde{\Phi} + \tilde{W}^T \hat{\Phi} + \hat{W}^T (\Phi_m \tilde{m} + \Phi_\sigma \tilde{\sigma} + \Phi_r \tilde{r} + o(\cdot)) + \xi \\ &= \tilde{W}^T \tilde{\Phi} + \xi + \hat{W}^T o(\cdot) + \tilde{W}^T \hat{\Phi} + \hat{W}^T \Phi_m \tilde{m} + \hat{W}^T \Phi_\sigma \tilde{\sigma} + \hat{W}^T \Phi_r \tilde{r} \end{aligned} \tag{21}$$

Define $\Theta = \tilde{W}^T \tilde{\Phi} + \xi + \hat{W}^T o(\cdot)$; since $\|\xi\| \leq \bar{\xi}$, it is assumed that Θ is bounded, and $\|\Theta\| \leq \mathfrak{I}$,

where \mathfrak{I} is a constant. Therefore,

$$\tilde{\delta} = \tilde{W}^T \hat{\Phi} + \hat{W}^T \Phi_m \tilde{m} + \hat{W}^T \Phi_\sigma \tilde{\sigma} + \hat{W}^T \Phi_r \tilde{r} + \Theta. \tag{22}$$

Theorem 4.1. For the nonlinear system (6) with bounded uncertainties, if the control

law is designed in the form of

$$u(t) = g^{-1}(x(t)) \left[-f(x(t)) + x_d^{(n)}(t) + \alpha^T E(t) - \hat{\delta} \right] + g^{-1}(x(t)) \hat{\mathfrak{I}} \operatorname{sgn}(s(t)), \tag{23}$$

and adaptive regulation law is adopted as

$$\begin{cases} \dot{\hat{W}} = -K_w s_l \hat{W} \\ \dot{\hat{m}} = -K_m \Phi_m^T \hat{W} s \\ \dot{\hat{\sigma}} = -K_\sigma \Phi_\sigma^T \hat{W} s \\ \dot{\hat{r}} = -K_\gamma \Phi_r^T \hat{W} s \\ \dot{\hat{\mathfrak{I}}} = K_{\mathfrak{I}} \|s\| \end{cases} \tag{24}$$

where $l = 1, 2 \dots n_R$, and $\hat{\mathfrak{I}}$ is the estimated value of \mathfrak{I} ; the robot walking system will be asymptotically stable.

Proof. By substituting the control law (30) into (7) $x^{(n)}(t) = f(x(t)) + g(x(t))u(t) + \delta(x(t))$, one can get

$$\begin{aligned} x^{(n)}(t) &= f(x(t)) - f(x(t)) + x_d^{(n)}(t) + \alpha^T E(t) - \hat{\delta} + \delta + \hat{\mathfrak{I}} \operatorname{sgn}(s(t)) \\ &= \alpha^T E(t) + \hat{\mathfrak{I}} \operatorname{sgn}(s(t)) + x_d^{(n)}(t) - \hat{\delta} + \delta \end{aligned} \tag{25}$$

that is,

$$\begin{aligned} \alpha^T E(t) + \beta \dot{E}(t) + \hat{\mathfrak{J}} \operatorname{sgn}(s(t)) - \hat{\delta} + \delta &= 0 \\ \dot{s}(t) &= -\hat{\mathfrak{J}} \operatorname{sgn}(s(t)) - (-\hat{\delta} + \delta) \end{aligned}$$

The Lyapunov stability theory is used to analyze the stability of the system, and the candidate Lyapunov function is selected as

$$\begin{aligned} V_R(s, \tilde{W}, \tilde{m}, \tilde{\sigma}, \tilde{\gamma}, \tilde{\mathfrak{J}}) &= \frac{1}{2} s^T s + \frac{1}{2K_w} \operatorname{tr}(\tilde{W}^T \tilde{W}) + \frac{1}{2K_m} \tilde{m}^T \tilde{m} + \frac{1}{2K_\sigma} \tilde{\sigma}^T \tilde{\sigma} + \frac{1}{2K_\gamma} \tilde{\gamma}^T \tilde{\gamma} + \frac{1}{2K_{\mathfrak{J}}} \tilde{\mathfrak{J}}^2 \\ \dot{V}_R(s, \tilde{W}, \tilde{m}, \tilde{\sigma}, \tilde{\gamma}, \tilde{\mathfrak{J}}) &= s^T \dot{s} + \frac{1}{K_w} \operatorname{tr}(\dot{\tilde{W}}^T \tilde{W}) + \frac{1}{K_m} \tilde{m}^T \dot{\tilde{m}} + \frac{1}{K_\sigma} \tilde{\sigma}^T \dot{\tilde{\sigma}} + \frac{1}{K_\gamma} \tilde{\gamma}^T \dot{\tilde{\gamma}} + \frac{1}{K_{\mathfrak{J}}} \tilde{\mathfrak{J}} \dot{\tilde{\mathfrak{J}}} \\ s^T \dot{s} &= s^T (-\hat{\mathfrak{J}} \operatorname{sgn}(s) - (-\hat{\delta} + \delta)) \\ &= s^T \left(-\hat{\mathfrak{J}} \operatorname{sgn}(s) - \left(\tilde{W}^T \hat{\Phi} + \hat{W}^T \Phi_m \tilde{m} + \hat{W}^T \Phi_\sigma \tilde{\sigma} + \hat{W}^T \Phi_r \tilde{r} + \Theta \right) \right) \\ &= -\hat{\mathfrak{J}} \|s\| - s^T \Theta - s^T \tilde{W}^T \hat{\Phi} - s^T \hat{W}^T \Phi_m \tilde{m} - s^T \hat{W}^T \Phi_\sigma \tilde{\sigma} - s^T \hat{W}^T \Phi_r \tilde{r} \end{aligned}$$

Considering the structural characteristics of RNNs, $\operatorname{tr}(\tilde{W}^T \dot{\tilde{W}}) = \sum_{l=1}^{nR} \tilde{w}_l^T \dot{\tilde{w}}_l$, and $s^T \tilde{W}^T \hat{\Phi} = \sum_{l=1}^{nR} s_l \tilde{w}_l^T \hat{\Phi}$, we can obtain that

$$\begin{aligned} \dot{V}_R(s, \tilde{W}, \tilde{m}, \tilde{\sigma}, \tilde{\gamma}, \tilde{\mathfrak{J}}) &= -K_{\mathfrak{J}} \|s\| - s^T \Theta - s^T \tilde{W}^T \hat{\Phi} - s^T \hat{W}^T \Phi_m \tilde{m} - s^T \hat{W}^T \Phi_\sigma \tilde{\sigma} - s^T \hat{W}^T \Phi_r \tilde{r} \\ &+ \frac{1}{K_w} \operatorname{tr}(\dot{\tilde{W}}^T \tilde{W}) + \frac{1}{K_m} \tilde{m}^T \dot{\tilde{m}} + \frac{1}{K_\sigma} \tilde{\sigma}^T \dot{\tilde{\sigma}} + \frac{1}{K_\gamma} \tilde{\gamma}^T \dot{\tilde{\gamma}} + \frac{1}{K_{\mathfrak{J}}} \tilde{\mathfrak{J}} \dot{\tilde{\mathfrak{J}}} \\ &= -\hat{\mathfrak{J}} \|s\| - s^T \Theta - \sum_{l=1}^{nR} s_l \tilde{w}_l^T \hat{\Phi} - s^T \hat{W}^T \Phi_m \tilde{m} - s^T \hat{W}^T \Phi_\sigma \tilde{\sigma} - s^T \hat{W}^T \Phi_r \tilde{r} \\ &+ \frac{1}{K_w} \sum_{l=1}^{nR} \tilde{w}_l^T \dot{\tilde{w}}_l + \frac{1}{K_m} \tilde{m}^T \dot{\tilde{m}} + \frac{1}{K_\sigma} \tilde{\sigma}^T \dot{\tilde{\sigma}} + \frac{1}{K_\gamma} \tilde{\gamma}^T \dot{\tilde{\gamma}} + \frac{1}{K_{\mathfrak{J}}} \tilde{\mathfrak{J}} \dot{\tilde{\mathfrak{J}}} \\ &= -\sum_{l=1}^{nR} \tilde{w}_l^T \left(s_l \hat{\Phi} - \frac{1}{K_w} \dot{\tilde{w}}_l \right) - K_{\mathfrak{J}} \|s\| + \frac{1}{K_{\mathfrak{J}}} \tilde{\mathfrak{J}} \dot{\tilde{\mathfrak{J}}} - s^T \Theta \\ &+ \tilde{m}^T \left(\frac{1}{K_m} \dot{\tilde{m}} - \Phi_m^T \hat{W}^T s \right) + \tilde{\sigma}^T \left(\frac{1}{K_\sigma} \dot{\tilde{\sigma}} - \Phi_\sigma^T \hat{W}^T s \right) + \tilde{\gamma}^T \left(\frac{1}{K_\gamma} \dot{\tilde{\gamma}} - \Phi_\gamma^T \hat{W}^T s \right) \end{aligned} \tag{26}$$

According to the basic principle of SMC, there is $s(t) \rightarrow 0$ when $t \rightarrow \infty$, thus, $\dot{\tilde{w}} = -\dot{\tilde{W}}, \dot{\tilde{m}} = -\dot{\tilde{m}}, \dot{\tilde{\sigma}} = -\dot{\tilde{\sigma}}, \dot{\tilde{\gamma}} = -\dot{\tilde{\gamma}}, \dot{\tilde{\mathfrak{J}}} = -\dot{\tilde{\mathfrak{J}}}$.

Let the upper bound error be defined as $\tilde{\mathfrak{J}} = \mathfrak{J} - \tilde{\mathfrak{J}}$; on the other hand, by substituting the adaptive regulation law (23) into (26), we can obtain that

$$\begin{aligned} \dot{V}_R(s, \tilde{W}, \tilde{m}, \tilde{\sigma}, \tilde{\gamma}, \tilde{\mathfrak{J}}) &= -\sum_{l=1}^{nR} \tilde{w}_l^T \left(s_l \hat{\Phi} - \frac{1}{K_w} K_w s_l \hat{W} \right) - \hat{\mathfrak{J}} \|s\| + \frac{1}{K_{\mathfrak{J}}} \tilde{\mathfrak{J}} K_{\mathfrak{J}} \|s\| - s^T \Theta \\ &+ \tilde{m}^T \left(\frac{1}{K_m} K_m \Phi_m^T \hat{W} s - \Phi_m^T \hat{W}^T s \right) + \tilde{\sigma}^T \left(\frac{1}{K_\sigma} K_\sigma \Phi_\sigma^T \hat{W} s - \Phi_\sigma^T \hat{W}^T s \right) + \tilde{\gamma}^T \left(\frac{1}{K_\gamma} K_\gamma \Phi_\gamma^T \hat{W} s - \Phi_\gamma^T \hat{W}^T s \right) \\ &= (\tilde{\mathfrak{J}} - \hat{\mathfrak{J}}) \|s\| - s^T \Theta \leq 0 \end{aligned} \tag{27}$$

Hence, from (41), it can be seen that the Lyapunov function is not increasing but bounded in its domain of definition; that is, $V_R(0) = V(s(0), \tilde{W}(0), \tilde{m}(0), \tilde{\sigma}(0), \tilde{\gamma}(0), \tilde{\mathfrak{J}}(0))$, and $V_R(t) = V(s(t), \tilde{W}(t), \tilde{m}(t), \tilde{\sigma}(t), \tilde{\gamma}(t), \tilde{\mathfrak{J}}(t))$.

Let $R(t) = (\|\Theta\| - \mathfrak{J})S(t)$. Considering $s(t)$ is bounded, there exists

$$\begin{aligned} R(t) &\leq \|\Theta\| - \mathfrak{J} \|s(t)\| \leq -\dot{V}_R(s, \tilde{W}, \tilde{m}, \tilde{\sigma}, \tilde{\gamma}, \tilde{\mathfrak{J}}). \\ \int_0^t R(t) dt &\leq -\int_0^t \dot{V}_R(s, \tilde{W}, \tilde{m}, \tilde{\sigma}, \tilde{\gamma}, \tilde{\mathfrak{J}}) dt = V_R(0) - V_R(t). \end{aligned} \tag{28}$$

Table 1. Configuration parameters of robots

Parameter	Torso length	Thigh length	Calf length	Trunk mass	Thigh mass	Calf length	Thigh rotational inertia	Calf rotational inertia
Value unit	0.204 m	0.412 m	0.385 m	5.9 kg	13.2 kg	7.7 kg	0.56 kgm ²	0.28 kgm ²

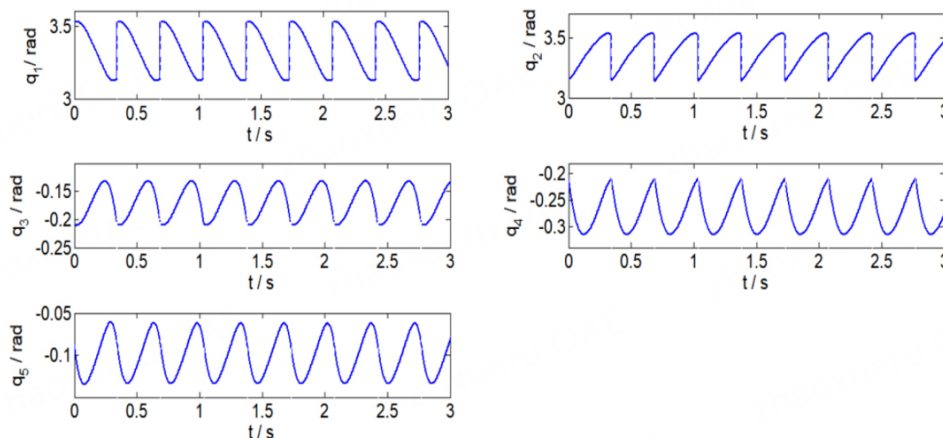


Figure 4. The absolute joint angles q_i vary with time.

According to the Barbat lemma, we obtain $\lim_{t \rightarrow \infty} R(t) = 0$; hence, the system can be asymptotically stable when $\lim_{t \rightarrow \infty} s(t) = 0$. This completes the proof of Theorem 1.

5. EXPERIMENTAL RESULTS AND DISCUSSION

To verify the control methods given in Section 3 and Section 4, simulations are implemented. The configuration parameters of robots are shown in Table 1.

Figure 4 shows that the absolute joint angles q_i vary with the time of the biped robot in the duration of walking. It shows that the phase of each joint is reset based on the foot contact information at the beginning of each step. The trajectories of each joint are smooth and periodic. q_1 and q_2 have a jump in every period, indicating the switch between the swing leg and support leg. Figure 4 illustrates a phase diagram of the joint angle q_i and joint angular velocity \dot{q}_i during the walking process, which are all limited circles to prove that the walking process can achieve asymptotic stability. In Figure 5, the straight lines indicate the discrete instance of the walking gait. It stands for the fact that the swinging leg has an impulsive action on the ground, and the joint angular velocity \dot{q}_i has a sudden change at the same time.

Figure 6 shows the total energy of the system changes over time in the body and inertial frame, respectively. Figure 7 shows the stride length. Figure 8 shows the hip position in the body and inertial frame, and its velocity is shown in Figure 9.

Let external disturbance $\tau_d = [\exp(-0.1t)]_{6 \times 1}$ be exerted on the link 2 when $t = 2.5$ s. This will lead to the changes of the inertia matrix, Coriolis force matrix, and gravity matrix of the robot system, which is equivalent to introducing the model uncertainty. Set the error upper bound $\beta = 1$, and the boundary layer thickness is set as 0.01. The simulation results are shown in Figure 10 and Figure 11.

Figure 10 depicts the tracking effect of each joint. The blue solid line and the red dotted line represent the actual position and desired position of each joint in the walking process, respectively. The simulation results

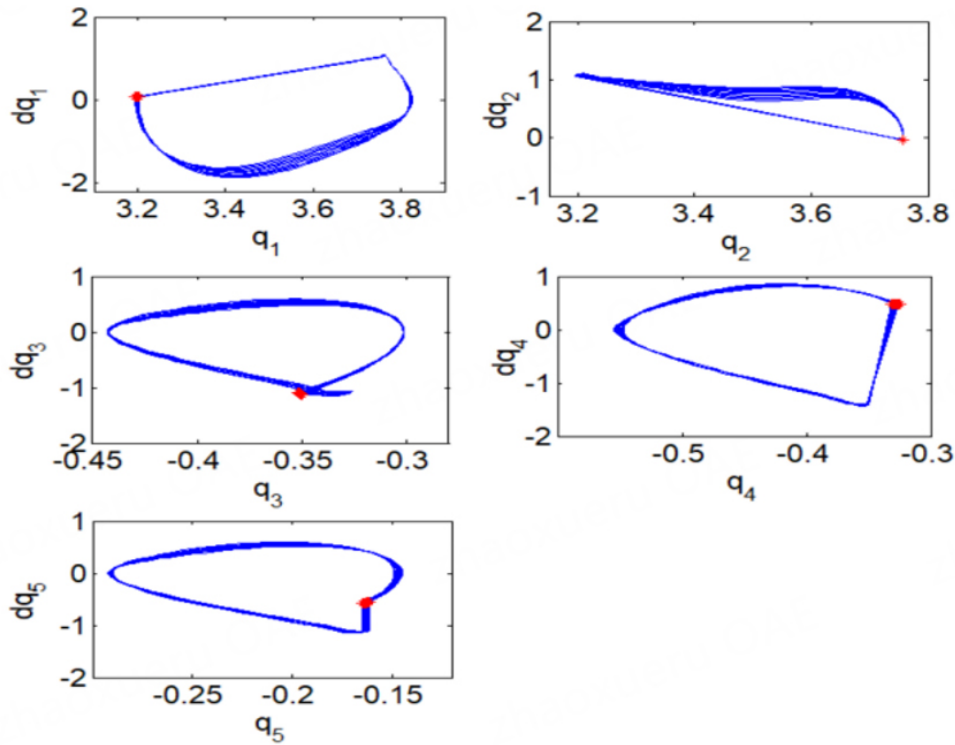


Figure 5. Phase diagram of joint angle q_i and joint angular velocity \dot{q}_i .

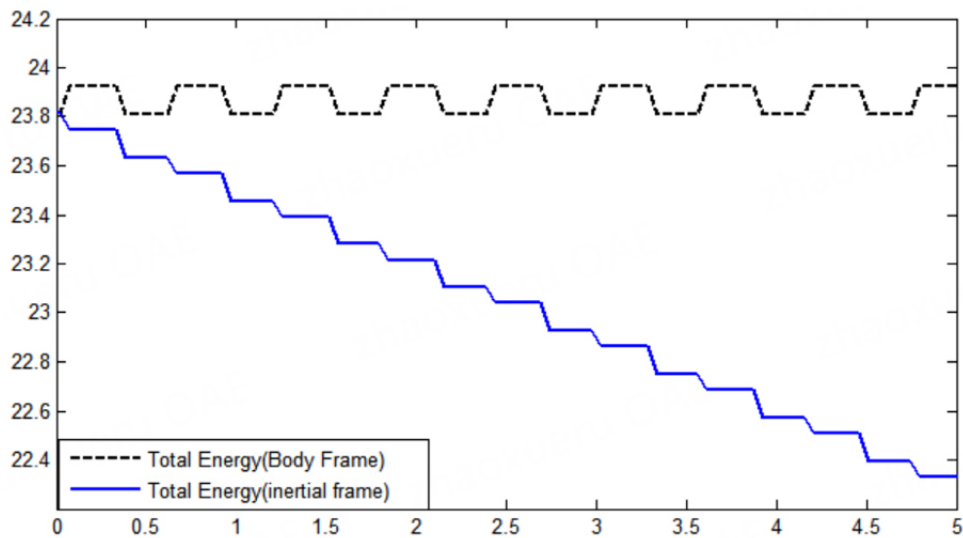


Figure 6. Energy plot.

show that satisfactory excessive control chattering exists due to the fault of mass change. It can be seen that the designed adaptive sliding mode controller can meet the tracking requirement of the desired trajectory. Figure 11 describes the comparisons of system input torque. The comparisons of joint errors with time are shown in Figure 12. It indicates that the joint error finally tends to 0, which shows that the system can converge to the sliding surface and the robot can realize asymptotically stable walking. These figures illustrate that the proposed adaptive SMC control system can achieve the purpose of tracking reference trajectories. Therefore, the tracking errors of the proposed RNN hybrid control system converge more quickly than without adaptive SMC.

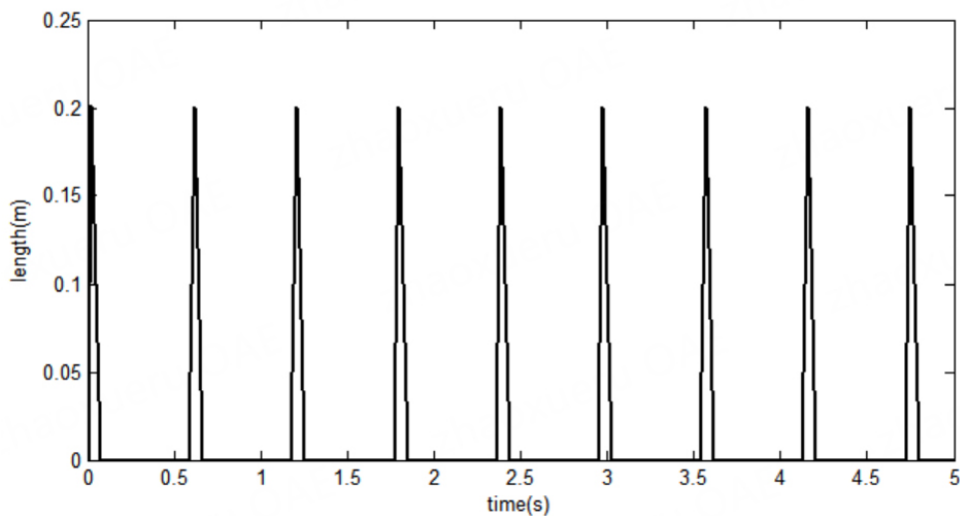


Figure 7. Stride length.

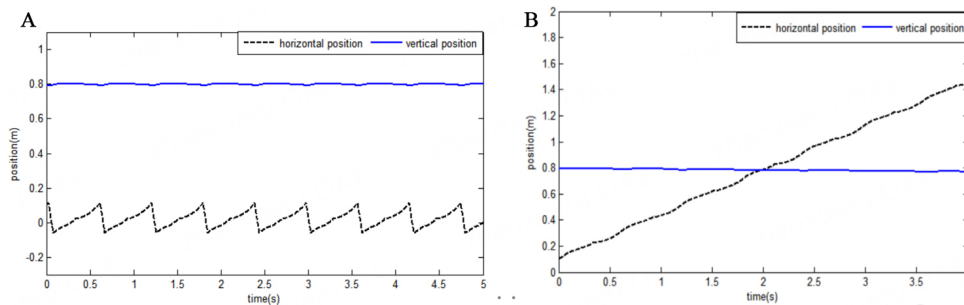


Figure 8. Hip position.

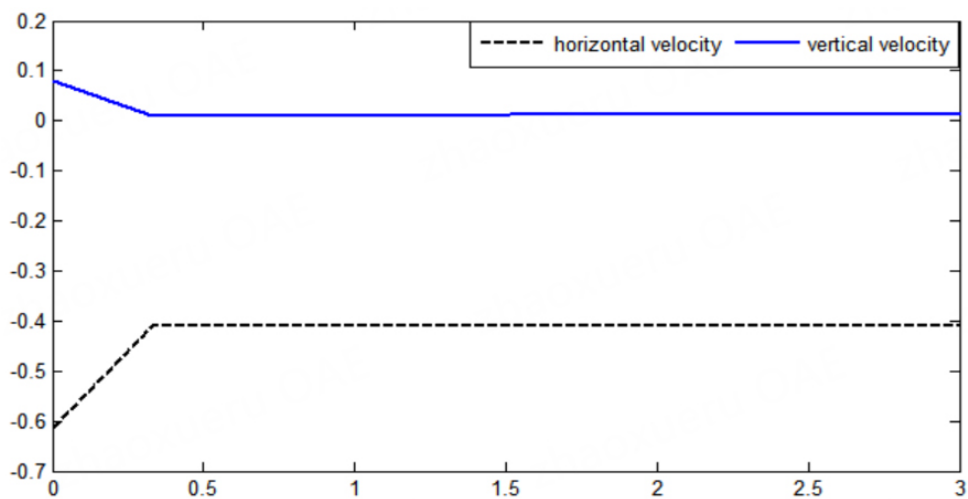


Figure 9. Hip velocity.

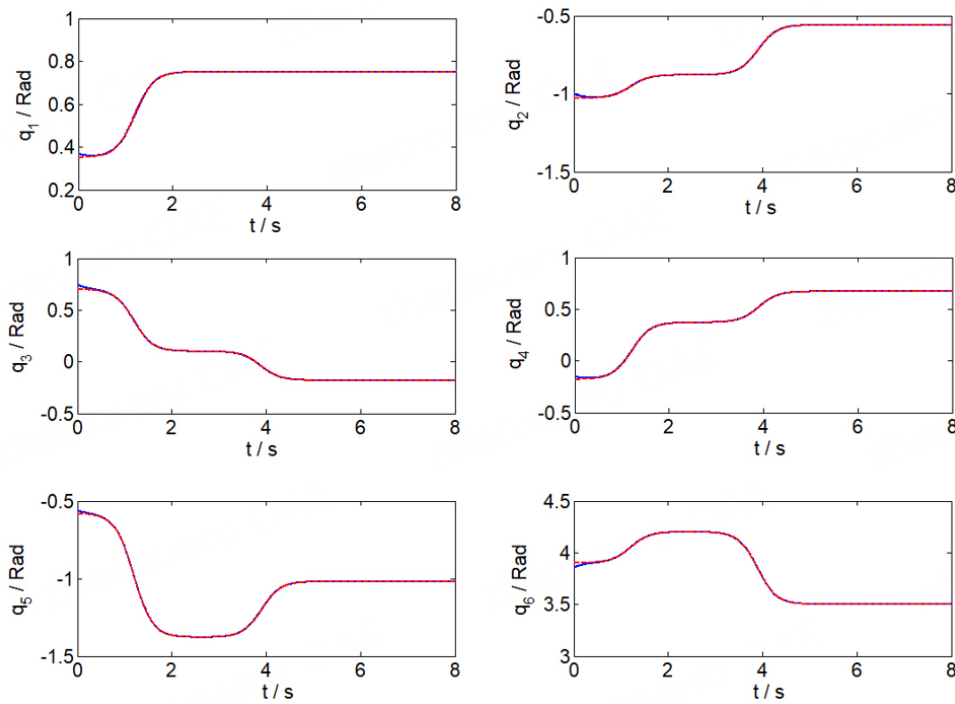


Figure 10. The tracking effect of joint motion in the adaptive sliding mode control (SMC).

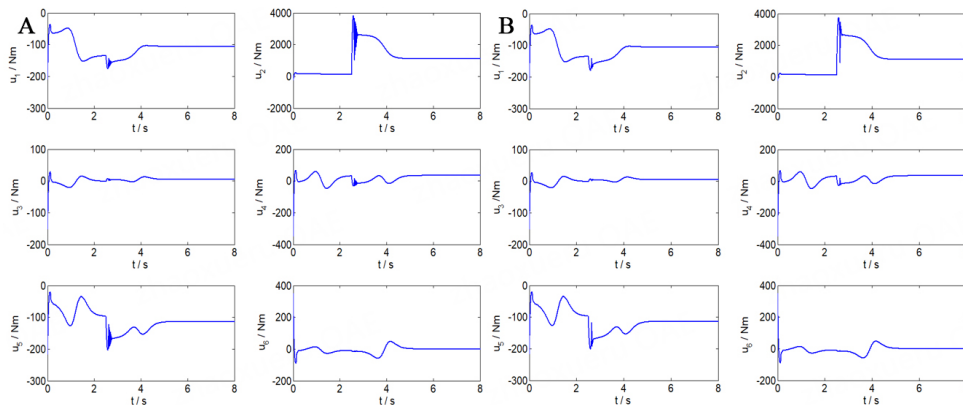


Figure 11. The comparisons of system input torque. (A) with adaptive sliding mode control (SMC); (B) without adaptive SMC.

6. CONCLUSIONS

The problem of external disturbance uncertainties will affect the stability during dynamic walking, which has greatly limited the application and efficiency of robots. In this paper, the robust and efficient walking of biped robots is investigated. The robust walking model will be optimized, which provides a theoretical basis for flexible and stable humanoid walking. The focus is on the following aspects: (1) analyzing the mechanism of disturbances and studying robust control strategies from the perspective of theoretical analysis; (2) transforming the target of stable biped walking into the problem of stabilization of periodic orbits and through stability analysis; (3) constructing the autonomous evolution mechanism based on hybrid robust control to realize adaptive optimization of walking models. The verification of the proposed control method is conducted by simulations. In future work, a more human-like walking gait will be designed to achieve more efficient walking. The external disturbance has been considered as an unknown uncertainty, and an uncertainty observer will be designed for efficient learning and dynamic response.

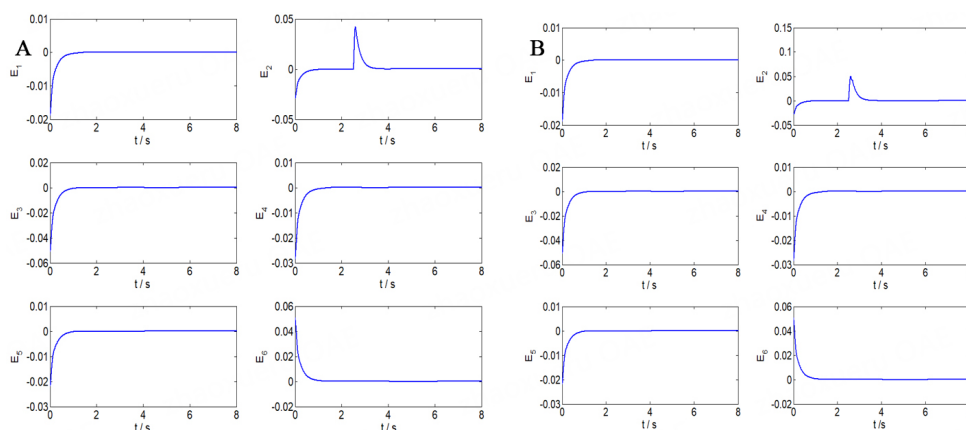


Figure 12. The comparisons of joint errors with time. (A) with adaptive sliding mode control (SMC); (B) without adaptive SMC.

DECLARATIONS

Authors' contributions

Made substantial contributions to the conception and design of the study and performed data analysis and interpretation: Wang H

Performed data acquisition and provided administrative, technical, and material support: Wang H, Chen Q

Availability of data and materials

Not applicable.

Financial support and sponsorship

This work is supported by the National Natural Science Foundation of China (No. 61733013; No. 61573260; No. 62073245; No. U1713211).

Conflicts of interest

All authors declared that there are no conflicts of interest.

Ethical approval and consent to participate

Not applicable.

Consent for publication

Not applicable.

Copyright

© The Author(s) 2023.

REFERENCES

1. Yang C, Jiang Y, Na J, Li Z, Cheng L, Su C. Finite-time convergence adaptive fuzzy control for dual-arm robot with unknown kinematics and dynamics. *IEEE Trans Fuzzy Syst* 2019;27:574-88. [DOI](#)
2. Liu C, Zhang T, Liu M, Chen Q. Active balance control of humanoid locomotion based on foot position compensation. *J Bionic Eng* 2020;17:134-47. [DOI](#)
3. Rus D, Tolley MT. Design, fabrication and control of soft robots. *Nature* 2015;521:467-75. [DOI](#)
4. Chen G, Xu Y, Yang C, et al. Design and control of a novel bionic mantis shrimp robot. *IEEE/ASME Trans Mechatron* 2023;online ahead of print. [DOI](#)
5. Qiang Huang, Yokoi K, Kajita S, et al. Planning walking patterns for a biped robot. *IEEE Trans Robot Automat* 2001;17:280-9. [DOI](#)
6. Tedrake R, Zhang TW, Seung HS. Stochastic policy gradient reinforcement learning on a simple 3D biped. In: 2004 IEEE/RSJ International Conference on Intelligent Robots and Systems; 2004 Sep 28 - Oct 02; Sendai, Japan. IEEE; 2004. p. 2849-54. [DOI](#)

7. Grizzle J, Abba G, Plestan F. Asymptotically stable walking for biped robots: analysis via systems with impulse effects. *IEEE Trans Automat Contr* 2001;46:51-64. [DOI](#)
8. Heydarnia O, Dadashzadeh B, Allahverdzadeh A, Sayyed Noorani MR. Discrete sliding mode control to stabilize running of a biped robot with compliant kneed legs. *Aut Control Comp Sci* 2017;51:347-56. [DOI](#)
9. Devi MA, Udupa G, Sreedharan P. A novel under-actuated multi-fingered soft robotic hand for prosthetic application. *Rob Auton Syst* 2018;100:267-77. [DOI](#)
10. Roberts D, Quacinella J, Kim JH. Energy expenditure of a biped walking robot: instantaneous and degree-of-freedom-based instrumentation with human gait implications. *Robotica* 2017;35:1054-71. [DOI](#)
11. Anjum MB, Khan Q, Ullah S, et al. Maximum power extraction from a standalone photo voltaic system via neuro-adaptive arbitrary order sliding mode control strategy with high gain differentiation. *Appl Sci* 2022;12:2773. [DOI](#)
12. Ugurlu B, Saglia JA, Tsagarakis NG, et al. Hopping at the resonance frequency: a trajectory generation technique for bipedal robots with elastic joints. In: IEEE International Conference on Robotics and Automation; 2012 May 14-18; Saint Paul, MN, USA. IEEE; 2012. p. 1436-43. [DOI](#)
13. Jeong SH, Kim K, Kim S. Designing anthropomorphic robot hand with active dual-mode twisted string actuation mechanism and tiny tension sensors. *IEEE Robot Autom Lett* 2017;2:1571-8. [DOI](#)
14. Labbadi M, Iqbal J, Djemai M, Boukal Y, Bouteraa Y. Robust tracking control for a quadrotor subjected to disturbances using new hyperplane-based fast Terminal Sliding Mode. *PLoS One* 2020;10:1635. [DOI](#)
15. Yadukumar SN, Pasupuleti M, Ames AD. Human-inspired underactuated bipedal robotic walking with AMBER on flat-ground, up-slope and uneven terrain. In: IEEE/RSJ International Conference on Intelligent Robots and Systems; 2012 Oct 07-12; Vilamoura-Algarve, Portugal. IEEE; 2012. p. 2478-83. [DOI](#)
16. Dai HK, Tedrake R. L2-gain optimization for robust bipedal walking on unknown terrain. In: IEEE International Conference on Robotics and Automation; 2013 May 06-10; Karlsruhe, Germany. IEEE; 2013. p. 3116-23. [DOI](#)
17. Ahmad S, Uppal AA, Azam MR, Iqbal J. Chattering free sliding mode control and state dependent kalman filter design for underground gasification energy conversion process. *Electronics* 2023;12:876. [DOI](#)
18. Or Y, Ames AD. Stability and completion of zeno equilibria in lagrangian hybrid systems. *IEEE Trans Automat Cont* 2011;56:1322-36. [DOI](#)
19. Lamperski A, Ames AD. Lyapunov theory for zeno stability. *IEEE Trans Automat Contr* 2013;58:100-12. [DOI](#)
20. Orlov Y. Finite time stability and robust control synthesis of uncertain switched systems. *SIAM J Control Optim* 2004;43:1253-71. [DOI](#)
21. Spong MW. The passivity paradigm in the control of bipedal robots. In: Climbing and walking robots. Berlin, Heidelberg: Springer; 2005. p. 775-86. [DOI](#)
22. Ravichandran MT, Mahindrakar AD. Robust stabilization of a class of underactuated mechanical systems using time scaling and lyapunov redesign. *IEEE Trans Ind Electron* 2011;58:4299-313. [DOI](#)
23. Sreenath K, Park HW, Grizzle JW. HDesign and experimental implementation of a compliant hybrid zero dynamics controller with active force control for running on MABEL. In: IEEE International Conference on Robotics and Automation; 2012 May 14-18; Saint Paul, MN, USA. IEEE; 2012. p. 51-6. [DOI](#)
24. Geng T, Porr B, Wörgötter F. Fast biped walking with a sensor-driven neuronal controller and real-time online learning. *Int J Rob Res* 2016;25:243-59. [DOI](#)
25. Su H, Qi W, Hu Y, Karimi HR, Ferrigno G, Momi ED. An incremental learning framework for human-like redundancy optimization of anthropomorphic manipulators. *IEEE Trans Ind Inf* 2022;18:1864-72. [DOI](#)
26. Kai T, Shintani TS. A discrete mechanics approach to gait generation on periodically unlevel grounds for the compass-type biped robot. *IJARAI* 2013;2:43-51. [DOI](#)
27. Yang C, Jiang Y, He W, Na J, Li Z, Xu B. Adaptive parameter estimation and control design for robot manipulators with finite-time convergence. *IEEE Trans Ind Electron* 2018;65:8112-23. [DOI](#)
28. Van M, Do XP, Mavrouniotis M. Self-tuning fuzzy PID-nonsingular fast terminal sliding mode control for robust fault tolerant control of robot manipulators. *ISA Trans* 2020;96:60-8. [DOI](#)
29. Kim Y, Lee J, Lee J. A balance control strategy for a walking biped robot under unknown lateral external force using a genetic algorithm. *Int J Human Robot* 2015;12:1550021. [DOI](#)
30. Wang H, Zhang H, Wang Z, Chen Q. Finite-time stabilization of periodic orbits for under-actuated biped walking with hybrid zero dynamics. *Commun Nonlinear Sci* 2020;80:104949. [DOI](#)